Pergamon

INTERNATIONAL JOURNAL OF MACHINE TOOLS & MANUFACTURE
DESIGN, RESEARCH AND APPLICATION

International Journal of Machine Tools & Manufacture 39 (1999) 965–983

Basic geometric analysis of 3-D chip forms in metal cutting. Part 2: implications

A. Kharkevich, Patri K. Venuvinod*

Department of Manufacturing Engineering and Engineering Management, City University of Hong Kong, Hong Kong

Received 8 May 1998

Abstract

The geometric analysis of 3-D chip forms developed in Part 1 is extended and several new implications are identified: (i) the geometric properties at every point on the tool–chip separation line are fully determined once those at any one point are known, (ii) all possible 3-D chip forms are confined to a relatively restricted parameter space defining the chip velocity direction and the orientation of the axis of the helical chip, (iii) 3-D helical chips are only approximately conical, and (iv) the radii of up-curl and side-curl can be determined from a set of simple measurements of the chip-in-hand. Unlike past analyses, the new analysis paves the way to the study of chip forms from empirical data obtained from practical 3-D chips. © 1999 Elsevier Science Ltd. All rights reserved.

Keywords: Up-curl; Side-curl; Helical chip; Chip forms; Metal cutting

The nomenclature listed in Part 1 [1] continues to be used in Part 2. The following lists only the additional nomenclature.

Nomenclature

b_1	slant width of helical chip; length of line joining C_0 and C_1
C	an arbitrary point on the FLASC
C_0, C_1	end point of the FLASC corresponding to the largest and the smallest chip radius respectively
f_0	the magnitude of f corresponding to point O_0
h_1	length of projection of b_1 on chip axis, A_H

* Corresponding author. Tel.: 00-852-2788-8400; Fax: 00-852-2788-8423; E-mail: mepatri@cityu.edu.hk

0890-6955/99/$ - see front matter
PII: S0890-6955(98)00066-2

k_1, k_2	constants defined in the text
l	the distance between points O_0 and O on the tool–chip separation line
l_1	length of the tool–chip separation line; distance O_0 O_1
O_0, O_1	end point of the TCSL generating helix $\mathbf{H}_0$ and $\mathbf{H}_1$ respectively
FLASC	face line of axial section of chip
α	angle between vectors $\boldsymbol{\rho}$ and $\boldsymbol{\rho}_0$
α_1	magnitude of α when $\boldsymbol{\rho}_1$ replaces $\boldsymbol{\rho}$
δ	length of the perpendicular from point C on to straight line C_0C_1
δ_m	the maximum value of δ
ρ_0, ρ_1	the largest and the smallest radius of screw chip face respectively
η_0, η_1	the magnitude of η at point O_0 and point O_1 respectively

1. Introduction

In Part 1 [1], the concept of 'lightly obstructed' chips was introduced. It was noted that initially continuous chips are born curled and may subsequently break because of external forces arising from an encounter with an obstacle (e.g. a tool or work surface) external to the chip formation zone. When the external forces are light, they merely modify the deformation pattern within the chip formation zone which, in turn, modifies the chip form as the chip leaves the cutting zone. The study of the generalized helical geometry of such lightly obstructed and unobstructed chips is basic to the study of most chip forms observed in metal cutting [1,2].

Whereas the majority of lightly obstructed and unobstructed chips obtained in practice are 3-D in nature, much of the literature available on chip curl has focused on the 2-D cases of pure up-curl and pure side-curl. Spaans [3] and Nakayama and Ogawa [4] pioneered the characterization of a 3-D chip form in terms of three parameters: up-curl radius, side-curl radius and chip flow angle. The prevailing approach towards 3-D chip form analysis is represented by Nakayama et al. [4,5]. These authors highlighted the importance of the tool–chip separation line (TCSL) in locating the chip helix, defined the radii of chip up-curl and side-curl, ρ_u and ρ_s respectively, and developed a set of basic equations governing 3-D chip geometry in terms of ρ, θ and η. However, it was found in Part 1 that the analysis given in [4,5] leads to some unsatisfactory results owing to inconsistencies related to the definition of ρ_u and ρ_s. Hence six plausible alternative hypotheses concerning the definitions of ρ_u and ρ_s were identified and each of these was tested against six criteria. It was found that only one (new) hypothesis (see Hypothesis 3 in Part 1) satisfied all the criteria. Further, although the works of Nakayama et al. had analysed 3-D chip geometry, these had not addressed the question of deriving the respective curl radii from measurements of 3-D chips-in-hand, i.e. measurements on 3-D chips *after* they have been separated from the cutting zone.

The present paper, Part 2, extends the analysis developed in Part 1 by addressing the issue of determining the radii of up-curl and side-curl, as well as the values of θ, η and e, from simple measurements of chips-in-hand obtained by cutting with tools with flat rake faces. In doing so, several hitherto unrecognized implications will be identified. Hence, each of the following sub-sections will start with a statement of the implication followed by an analytical justification of the statement.

2. Discovery of implications

2.1. Implication 1: the geometric properties at every point on the TCSL are determined once those at any one point have been determined

Since the focus in Part 1 was on the general point O on the TCSL and the associated helix, **H**, the analysis was carried out with reference to the Cartesian system XYZ centred at point O. In contrast, the following analysis aims to predict the geometry of the entire face (the screw surface referred to in Part 1) of the chip by viewing it as a collection of helices $\mathbf{H}_0$ to $\mathbf{H}_1$. In order to meet this aim, we will assume that the basic parameter set (ρ_0, η_0, θ) corresponding to the outer separation point O_0 is known and attempt to determine the geometric properties at an arbitrary point, O, which is at a given distance l from O_0 along the straight TCSL (see Fig. 1). Note that we need to determine only ρ and η since the magnitude of θ is the same for every chip helix. In order to facilitate further analysis, we will re-position the XYZ system to be centred at O_0 while retaining the axis orientations. This re-positioning has no effect on the various equations developed in Part 1.

Now, it can be shown from Fig. 1 that

$$f = f_0 - l\sin\theta \tag{1}$$

Combining Eq. 12 in [1] with the conclusion in Part 1 that the magnitude e is the same for every point on the TCSL, i.e. $e_0 = e$, it can be shown that

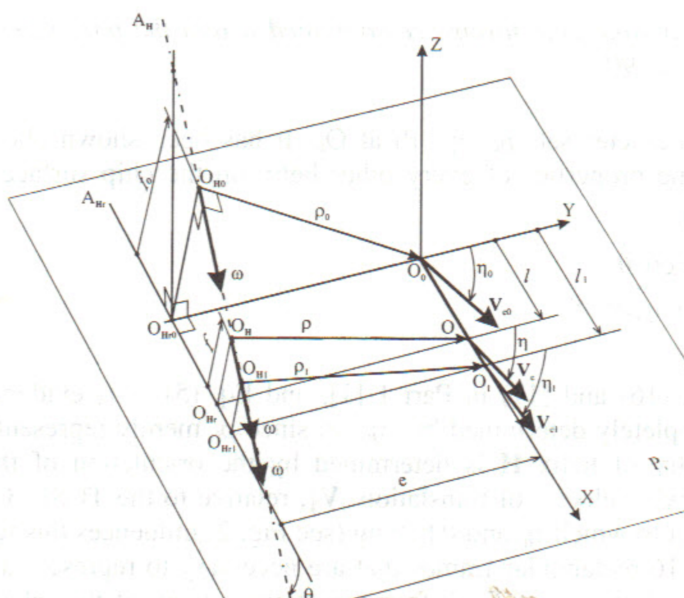

Fig. 1. Geometric analysis of 3-D helical chip form parameters along TCSL.

$$\rho = \rho_0 \frac{\sin\eta_0\sqrt{1 - \sin^2\eta\cos^2\theta}}{\sin\eta\sqrt{1 - \sin^2\eta_0\cos^2\theta}} \tag{2}$$

Combining Eq. (13) in [1], Eq. (1) and Eq. (2),

$$\cot\eta = \cot\eta_0 - \frac{l\sin\theta\sqrt{1 - \sin^2\eta_0\cos^2\theta}}{\rho_0\sin\eta_0} \tag{3}$$

Since the chip body is assumed to be rigid, the velocity of translation $\mathbf{V}_T$ of all the chip particles is the same. Thus, from Eq. (3) in [1] it follows that

$$V_c = V_{c0}\sin\eta_0/\sin\eta \tag{4}$$

Note that Eq. (3) determines η explicitly for an arbitrary point of the TCSL specified by a certain value of l. Substituting this value of η into Eq. (2), we can immediately determine ρ. Finally, applying Eq. (4), we can determine V_c. Evidently, although Eqs. (1)–(4) express the specific parameters belonging to an arbitrary point O in terms of those belonging to point O_0, similar forms of equations are obtained with regard to any two points on the TCSL. Therefore, it may be concluded that once the basic parameter set, (ρ, η, θ), and V_c at any point on the TCSL have been determined, the corresponding parameters at any other point (specified by the corresponding value of l) on the TCSL are automatically determined. Likewise, every helix on the chip surface is automatically determined once any one of the helices has been determined.

2.2. *Implication 2: all possible chip forms are contained within the parameter space $90° \leq \theta \leq 90°$ and $-90° \leq \eta_0 \leq 90°$*

Consider the basic parameter set (ρ_0, η_0, θ) at O_0. It has been shown above that this set is adequate to determine the properties of every other helix on the chip surface. Combining Eqs. (3) and (7) in Part 1 [1]

$$V_T = \rho_0\omega \frac{\sin\eta_0\cos\theta}{\sqrt{1 - \sin^2\eta_0\cos^2\theta}} \tag{5}$$

From Eqs. (12), (13), (16) and (17) in Part 1 [1], and Eq. (5), it is evident that the form of the chip helix $\mathbf{H}_0$ is completely determined by (η_0, θ) since ρ_0 merely represents the scale factor.

Similarly, the geometry of helix $\mathbf{H}$ is determined by the orientation of the helix's angular velocity, $\boldsymbol{\omega}$, and the helix's velocity of translation, $\mathbf{V}_T$, relative to the TCSL. Consider now how the choice of the quadrant to which η_0 and θ belong (see Fig. 2) influences this relative orientation.

Fig. 2 is divided into 16 rectangular frames that are necessary to represent all possible combinations of the quadrants of η_0 and θ. Each frame contains a view of the rake face and the part of the chip adjacent to the TCSL as seen from a location above the rake face, i.e. as viewed from the positive side of Z-axis. The views have been obtained on the basis of the relevant expressions

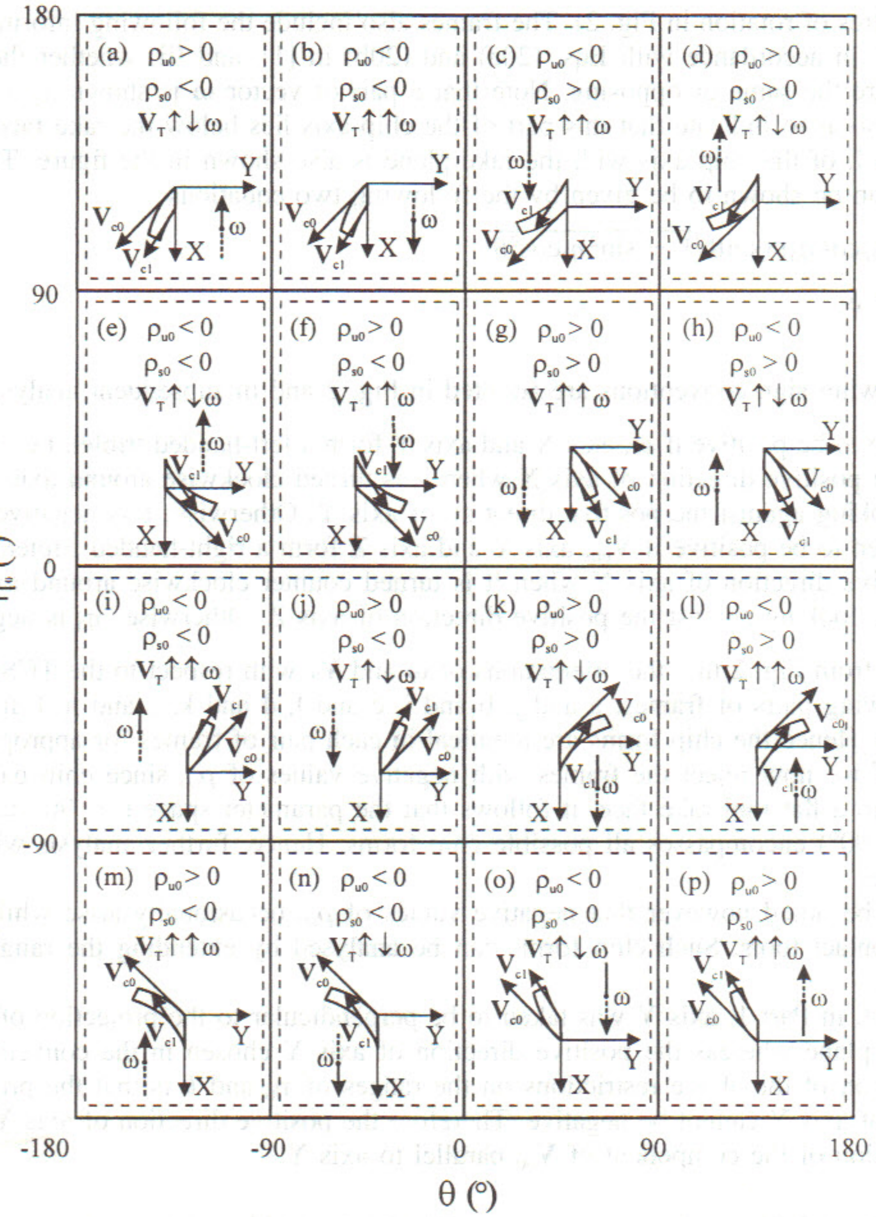

Fig. 2. Chip form features in the different quadrants of the circle range of η_0 and θ.

derived in Part 1 [1]. The view and the associated conditions shown in each frame are representative of the actual view and conditions everywhere within the frame except at the boundary of the frame. Each view represents the following information specified relative to axes X and Y: (i) the orientation of chip side curl; (ii) the TCSL, i.e. line O_0O_1; (iii) the velocities $\mathbf{V}_0$ and $\mathbf{V}_1$; (iv) the sliding vector of the angular velocity of rotation, $\boldsymbol{\omega}$, of the chip particles (for convenience of presentation, unlike in Fig. 1, the angular velocity vector has not been transported to the instantaneous centres of rotation in Fig. 2). The frames also include the following information: (i) signs of ρ_u and ρ_s in accordance with Eqs. (20a) and (20b) in [1], and (ii) whether the directions of $\mathbf{V}_T$ and $\boldsymbol{\omega}$ are the same or opposing. Note that a part of vector $\boldsymbol{\omega}$ is shown as a broken line in each frame so as to indicate that this part of the chip axis lies below the rake face. The point of intersection, I, of the chip axis with the rake plane is also shown in the figure. The coordinates of point I can be shown to be given by the following two equations

$$x_I = (\rho_0 \cos\eta_0)/(\sin\theta\sqrt{1 - \sin^2\eta_0 \cos^2\theta}) \tag{6}$$

$$y_I = -e \tag{7}$$

The following sign conventions are adopted in Fig. 2 and in subsequent analysis:

1. θ is taken to be positive if $\boldsymbol{\omega}$, axis X and axis Y form a left-handed triplet, i.e. if $\boldsymbol{\omega}$ is directed along the positive direction of axis X when it is turned clockwise around axis Y by angle $|\theta|$ while looking against the positive direction of axis Y. Otherwise, θ is negative.
2. η_0 is taken to be positive if $\mathbf{V}_{c0}$, axis Y and axis Z form a right-handed triplet, i.e. if $\mathbf{V}_{c0}$ has the positive direction of axis Y when it is turned counter clockwise around axis Z by angle $|\eta_0|$ while looking against the positive direction of axis Z. Otherwise, η_0 is negative.

It is seen from Fig. 2 that the orientations of $\boldsymbol{\omega}$ and $\mathbf{V}_T$ with respect to the TCSL are identical in the following pairs of frames: a and j, b and i, c and l, d and k, e and n, f and m, g and p, and h and o. Hence the chip forms are identical in each pair of frames for appropriate values of η_0 and θ. If we now reject the frames with negative values of ρ_{u0} since chip particles can not penetrate into a flat tool rake face, it follows that the parameter space ($-90° \leq \eta_0 \leq 90°$, $-90° \leq \theta \leq 90°$) encompasses all possible chip forms. Hence, further analysis will be confined to this range.

It should be noted however that negative values of ρ_{u0} occasionally arise while cutting with restricted contact tools. Such chip forms can be analysed by extending the range of θ to [$-180°$, $180°$].

Recall that, in Part 1, axis Y was taken to be perpendicular to the projection of the helix axis on the rake plane whereas the positive direction of axis Y chosen in the conventional manner. An implication of the above restrictions on the ranges of η_0 and θ is that the projection of $\mathbf{V}_{c0}$ on the line of axis Y cannot be negative. Therefore the positive direction of axis Y will be taken as the direction of the component of $\mathbf{V}_{c0}$ parallel to axis Y.

2.3. Implication 3: the parameter space (η_0, θ) of the possible chips becomes increasingly restricted with increasing relative chip width, $|l_1|/\rho_0$, along the TCSL

Consider the application of Eq. (3) to the other extreme point of the TCSL, O_1, where $\eta = \eta_1$. It follows from Eq. (20a) in Part 1 [1] that $\cos\eta_1$ has to be positive if ρ_{u1} were to be positive. In other words, just as with η_0 (see Implication 2), η_1 must be in the range [$-90°$, $90°$]. Further, Eq. (3) indicates that (i) $|\eta_1| \geq |\eta_0|$ which means that the difference between $|\eta_1|$ and $|\eta_0|$ increases when $|l_1|/\rho_0$ increases, and (ii) η_1 and η_0 have the same sign. Thus, clearly, if $|\eta_1| \in [-90°, 90°]$ then the range of η_0 must be smaller than [$-90°$, $90°$] when $|l_1|/\rho_0 > 0$. In fact, it can be shown that the application of the constraint ($\cos\eta_1 \geq 0$) to the relationship between η_1 and η_0 as derived from Eq. (3) leads to the observation that the following condition governing η_0 must be satisfied if the up-curl radius is to be positive everywhere on the TSCL of a 3-D chip:

$$|\eta_0| \leq \cot^{-1}\frac{|l_1\sin\theta|\sqrt{1-\sin^2\eta_0\cos^2\theta}}{\rho_0\sin|\eta_0|} \tag{8}$$

After appropriate transformation to eliminate η_0 from the right side of inequality Eq. (8), it can be shown that the maximum possible magnitude, $|\eta_0|_{max}$, of $|\eta_0|$ is given by

$$|\eta_0|_{max} = \cot^{-1}\frac{|\sin\theta|}{\sqrt{\left(\frac{\rho_0}{l_1\sin\theta}\right)^2 - 1}} \tag{9}$$

Fig. 3 shows the variation of $|\eta_0|_{max}$ with $|l_1|/\rho_0$ and $|\theta|$ as implied by the above up-curl constraint. It may be noted that, for a given outer chip radius, ρ_0, the maximum permissible magnitude of $|\eta_0|$ decreases with increasing values of $|\theta|$ and the chip width, $|l_1|$, along the TCSL. Likewise, for a given ρ_0, the maximum permissible magnitude of $|\theta|$ decreases with increasing values of $|\eta_0|$ and $|l_1|$. Therefore it is clear that the growth of $|l_1|/\rho_0$ imposes an increasingly tighter restriction on the feasible ranges of parameters η_0 and θ.

In particular, if $|\eta_0| = 90°$ and $\theta \neq 0$ then $l_1 = 0$ [see Eq. (9)], i.e. such a chip will have zero width. Further, if $\theta = 0$ and $|\eta_0| = 90°$ then $\eta_1 = \eta_0$ [Eq. (3)], $V_{R0} = V_{R1} = 0$ [Eq. (6) in Part 1 [1]], and $\mathbf{V}_{c0} = \mathbf{V}_{T0} = \mathbf{V}_{T1} = \mathbf{V}_{c1}$. Thus it follows that the chip particles at O_0 and O_1 of the TSCL under $|\eta_0| = 90°$ and $\theta = 0$ have just identical translational movements along the TSCL. Consequently such a chip also has zero width. Because of these considerations, $|\eta_0|$ will always be smaller than 90° for a real chip.

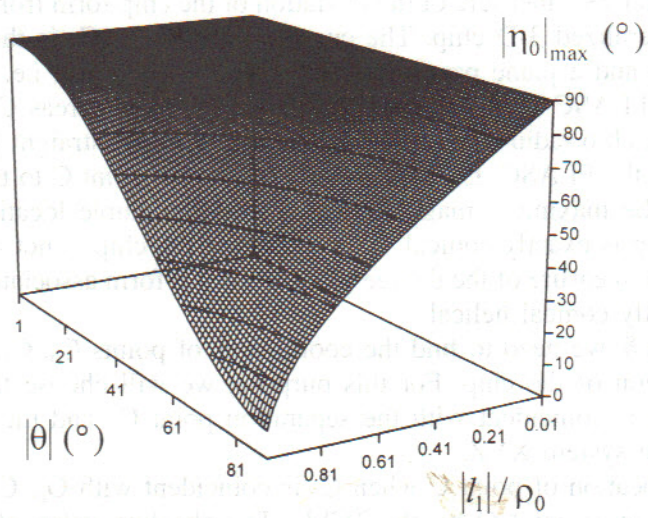

Fig. 3. The restriction on the maximum absolute value of η_0.

2.4. Implication 4: 3-D helical chips are only approximately conical, i.e. the chip axial section always has a slightly convex face line

Consider a generalized 3-D chip, i.e. a chip with $|\theta|\neq 0$, 90° and $\eta_0\neq 0$. The curl of such a chip may be said to be 'mixed' since the up-curl and side-curl radii are not of infinite magnitude. The pitch of the chip is not equal to zero. Further, the external and internal radii (ρ_0 and ρ_1 respectively) of the chip face are not equal and the difference between them is smaller than the chip width.

The straight TCSL is the generatrix of the chip face form. The shortest distance between the chip axis, A_H, and the TCSL is equal to $|e|$. According to Eq. (12) in Part 1 [1], $e = 0$ when $|\theta|\neq 0$ or 90° only if $\eta_0 = 0$. In this case the chip axis intersects the infinite straight line corresponding to the TCSL and hence the axis and the TCSL lie in the same plane. In such a situation, a rotation of the TCSL around the chip axis (directrix) generates a conical chip face. Such a chip is truly conical and has $V_T = 0$ so that the pitch is equal to zero. The face line of an axial section of the chip (FLASC) is straight in the case of such a chip.

Consider now the conditions to be satisfied if we wish to obtain a *truly* conical helical chip. To be conical it must have a straight-line segment as the FLASC. To be helical it should have a pitch of non-zero magnitude. In order to satisfy these conditions, suppose we start with a truly conical chip of zero pitch and impart to the generatrix of its face an additional translational motion (corresponding to $V_T\neq 0$) along the directrix so that we end up with the desired conical helical chip. However, this addition will cause η_0 and e to assume non-zero magnitudes. This means that the chip axis will move away from the TCSL. In other words, the condition of co-planarity between the generatrix and the directrix, which is necessary if the chip face were to be conical helical, is no more satisfied.

It follows from the above discussion that a truly conical helical chip does not exist although the term 'conical helical' has often been used in metal cutting literature (see e.g. [2,3]). Hence it is useful to estimate the error associated with the assumption of a conical helical chip. If the chip were indeed conical helical, the FLASC would be straight. Therefore, the straightness error of the FLASC may be taken as a measure of the deviation of the chip form from being conical helical.

Fig. 4 shows a generalized 3-D chip. The curve joining C_0 to C_1 is the curve of intersection between the chip face and a plane passing through the chip axis A_H, i.e. the FLASC. C_0 is the extreme point on the FLASC with the largest chip radius, ρ_0, whereas C_1 is the other extreme point with the smallest chip radius, ρ_1. Let b_1 be the length of the straight line joining C_0 and C_1.

Let C be a point on the FLASC. Let δ be the distance from point C to the straight-line joining C_0 to C_1. Let δ_m be the maximum magnitude of δ for all possible locations of point C on the FLASC. When the chip is exactly conical, $\delta_m = 0$. When the chip is not conical, $\delta_m \neq 0$. Thus, δ_m/b_1 may be taken as a measure of the degree of error in chip form associated with the assumption that the chip is perfectly conical helical.

In order to estimate δ, we need to find the coordinates of points C_0, C_1, and C with reference to an axial plane section of the chip. For this purpose, we will choose the axial plane passing through O_0 so that C_0 is coincident with the separation point O_0 and the coordinates of C_0 are (0,0,0) in the Cartesian system XYZ.

Now consider the location of point C when C_0 is coincident with O_0. C can be taken as lying on helix **H** generated by a point O on the TCSL. The absolute value of angle α between the radius vectors of rotation, $\boldsymbol{\rho}$ and $\boldsymbol{\rho}_0$, at O and O_0 respectively can be expressed as

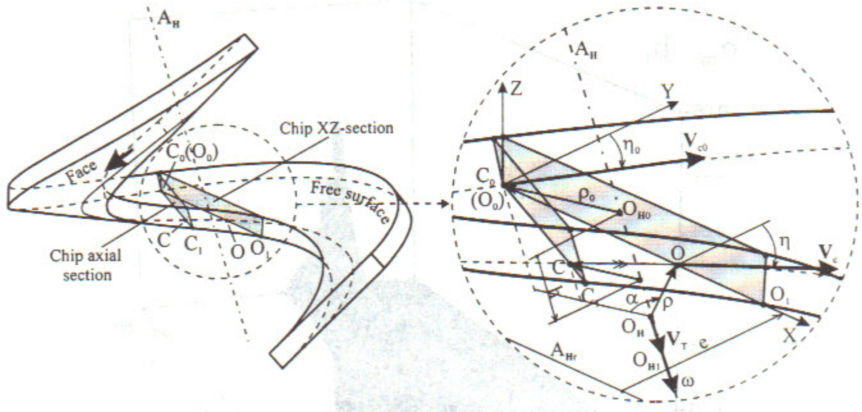

C_0CC_1 - FLASC
O_0OO_1 - TCSL

Fig. 4. Analysis of FLASC via TCSL.

$$|\alpha| = \cos^{-1}\frac{\boldsymbol{\rho}\cdot\boldsymbol{\rho}_0}{\rho\rho_0} = \cos^{-1}\frac{1 - \dfrac{l\sin\theta\cos\eta_0}{\rho_0\sqrt{1-\sin^2\eta_0\cos^2\theta}}}{\sqrt{1 - \dfrac{2l\sin\theta\cos\eta_0}{\rho_0\sqrt{1-\sin^2\eta_0\cos^2\theta}} + \left(\dfrac{l\sin\theta}{\rho_0}\right)^2}} \tag{10}$$

In order to determine the position of point C, we need to rotate vector ρ by angle $|\alpha|$ in the direction opposite to the angular velocity, ω, about axis $A_{\mathbf{H}}$ and translate the resulting point by distance $(V_T|\alpha|/\omega)$ in the direction opposite to the translational velocity $\mathbf{V}_T$ parallel to $A_{\mathbf{H}}$. When $l = l_1$, evidently, the location of C_1 is determined and the equation for the straight-line joining C_0 to C_1 is identified. It is a straightforward exercise to develop a numerical procedure for (i) determining the distance, δ, from point C to line C_0C_1, (ii) estimating the maximum magnitude, δ_m, of δ, and (iii) locating the position of C on the FLASC where δ assumes the maximum magnitude. Note that in these calculations a positive δ indicates that point C is on the side of line C_0C_1 that is away from the chip axis. Fig. 5 shows the result thus obtained for the case of $b_1/\rho_0 = 0.3$. There is an empty area of the $(|\eta_0|, |\theta|)$-space in Fig. 5 because this area corresponds to $\rho_{u1} \leq 0$ and therefore has been excluded from the analysis. It may be stated that δ (for a point inside the FLASC) and δ_m are always positive for general chips thus indicating that the FLASC is convex towards the outside of the chip. Thus, strictly speaking, mixed chips are not conical. While calculations show that a smaller value of b_1/ρ_0 leads to a smaller δ_m/b_1, the maximum value of δ_m/b_1 reached in Fig. 5 is only 6% even though b_1/ρ_0 has been set at the large value of 0.3. Therefore, the degree of deviation of a practical mixed 3-D chip from being strictly conical helical is very small.

Finally, it is not surprising, that the chips are not exactly conical when we recognize that a straight-line segment (TCSL) which is not placed on a plane containing the axis, $A_{\mathbf{H}}$, of generation has generated a chip face and FLASC. What is surprising is the observation that the FLASC is convex instead of being concave as one would expect when a distant oblique straight-line rotates

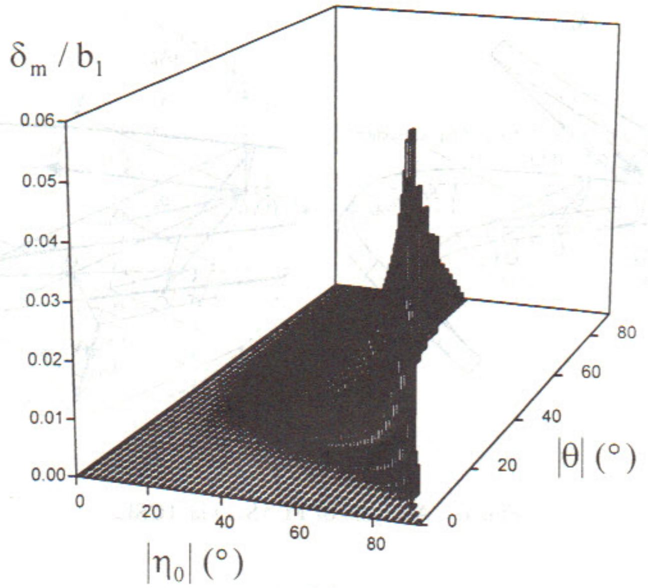

Fig. 5. Maximum straightness error of FLASC, δ_m/b_1.

about an axis. The reason for this unexpected result lies in the translation of such a generatrix along the axis of generation (directrix), $\mathbf{A_H}$, which is quick enough to invert the concavity caused by the rotation.

2.5. Implication 5: the magnitudes of ρ_u, ρ_s, and other analytical parameters are determinable from four simple measurements of the chip-in-hand

Fig. 6 illustrates a chip-in-hand, i.e. a chip that has been separated from the cutting zone. In the following, we aim to develop a procedure for determining ρ_u, ρ_s, etc., from an inspection and measurement of such a chip.

The magnitudes of ρ_u and ρ_s for the outer border of the chip face, i.e. ρ_{u0} and ρ_{s0}, can be determined from known magnitudes of ρ_0, η_0 and θ by substituting ρ by ρ_0 and η by η_0 in Eqs. (20a) and (20b) in Part 1 [1]. However, of these parameters, only ρ_0 can be measured off a chip-in-hand.

The first step in estimating the magnitudes of η_0 and θ is to determine the signs of these two parameters since we have already established that all possible chip forms are confined to the ranges $-90° \leq \theta \leq 90°$ and $-90° < \eta_0 < 90°$. Fig. 7 shows the computer simulations of the typical views that are obtained when the chip is placed on a horizontal surface and viewed from the top (the configurations shown were simulated for $|\eta_0| = |\theta| = 45°$). It is apparent that we can uniquely determine the signs of η_0 and θ by finding a match between the chip-in-hand and the configuration in one of the four quadrants in Fig. 7. Note that each configuration shows the inner and outer boundaries of the projection of the chip face. In addition, the points at which these boundaries are furthest away from the chip axis are marked. These are in fact the extreme points of the traced FLASC which correspond to the chip axial section in the viewing plane.

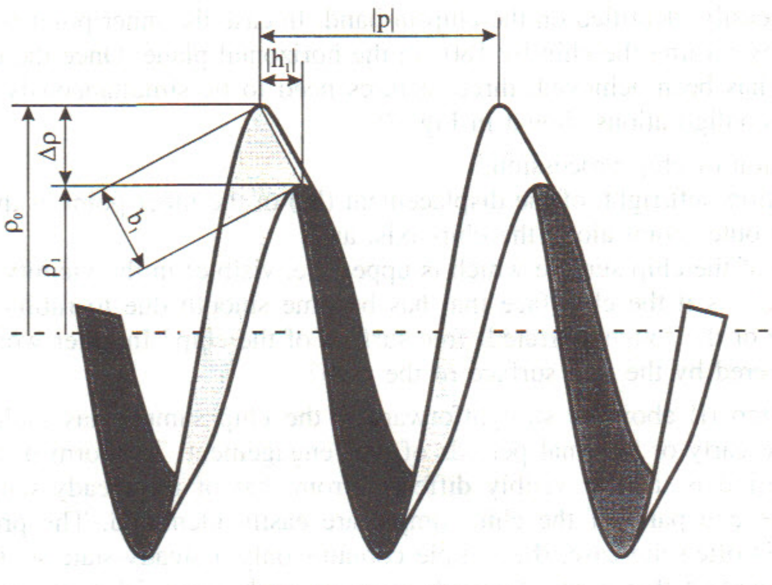

Fig. 6. A chip-in-hand.

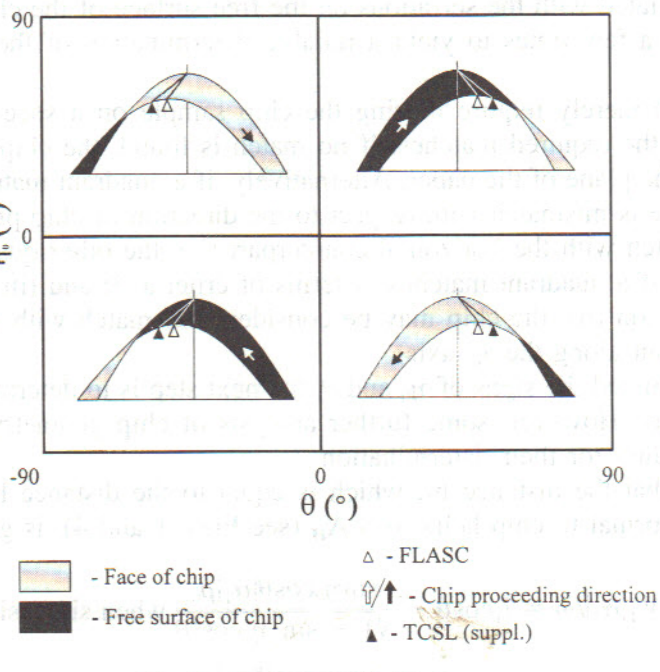

Fig. 7. Four principal chip forms.

These points are easily identified on the chip-in-hand. In case the inner point is not visible, it can be made visible by turning the chip by 180° in the horizontal plane. Once the correct position of the chip-in-hand has been achieved, three features need to be simultaneously matched between the chip and the configurations shown in Fig. 7:

(i) The direction of chip procession,
(ii) The direction, left/right, of the displacement (h_1) of the inner point of the FLASC relative to the similar outer point along the chip axis, and
(iii) The type of the chip surface which is upper (i.e. visible) in the vicinity of the inner point of the FLASC—is it the chip face that has become smooth due to rubbing action with the tool rake face or the rough (serrated) free surface of the chip? In other words, is the FLASC visible or covered by the free surface of the chip?

Carrying out step (i) above is straightforward if the chip sample has included the segment formed during the early or the final periods of tool engagement. The form of the chip produced during such a period is usually visibly different from that of the steady-state chip. Thus, the beginning and the end parts of the chip sample are easily identified. The procedure is not so simple when, as is often the case, the sample contains only a steady-state segment. The authors have found one method that seems to work in many such cases. This involves breaking off a small piece of the chip sample at one end by local bending directed such that the chip free surface undergoes tension and then examining the orientation of the broken cross section of the main part of the chip. Experience shows that the broken surface is usually inclined to the chip face (the chip surface that had undergone rubbing with the tool rake face) and the direction of this inclination coincides with the direction of chip procession. The reasons for this preferred orientation appear to lie in the orientation of elongated grains in the chip material and/or the orientation of shear bands associated with the serrations on the free surface of the chip. The procedure may need to be repeated a few times to yield a reliable determination of the direction of chip procession.

Steps (ii) and (iii) merely require placing the chip sample on a sheet of paper and visually inspecting it to find the required matches. If no match is found, the chip sample may be turned by 180° parallel to the plane of the paper. Alternatively, if a quadrant matches in terms of criteria (ii) and (iii) but there is mismatch with respect to the direction of chip procession, the chip may be considered to match with the horizontal counterpart (i.e. the other quadrant along the θ-axis) in Fig. 7. Similarly, if a quadrant matches in terms of criteria (i) and (iii) but there is mismatch with respect to criterion (ii), the chip may be considered to match with the vertical counterpart (i.e. the other quadrant along the η_0-axis).

Having thus determined the signs of η_0 and θ, the next step is to determine the absolute values of the two parameters. However, some further analysis of chip geometry is needed before one can identify a procedure for their determination.

It can be shown that the distance h_1, which is equal to the distance between planes passing through C_0 and C_1 normal to chip helix axis $A_{\mathbf{H}}$ (see Figs. 1 and 4), is given by

$$h_1 = \begin{vmatrix} l_1\cos\theta - V_T|\alpha_1|/\omega = l_1\cos\theta - \dfrac{\sin\eta_0\cos\theta|\alpha_1|\rho_0}{\sqrt{1-\sin^2\eta_0\cos^2\theta}} \text{ when } \sin\eta_0\sin\theta \geq 0 \\ l_1\cos\theta + V_T|\alpha_1|/\omega = l_1\cos\theta + \dfrac{\sin\eta_0\cos\theta|\alpha_1|\rho_0}{\sqrt{1-\sin^2\eta_0\cos^2\theta}} \text{ when } \sin\eta_0\sin\theta \leq 0 \end{vmatrix} \tag{11}$$

where the magnitude of $|\alpha_1|$ is determined by substituting $l = l_1$ in Eq. (10).

Replacing η, ρ and l in Eq. (3) by η_1, ρ_1 and l_1 respectively and rearranging

$$\frac{l_1\sin\theta}{\rho_0} = \frac{-(\sin\eta_0/\tan\eta_1) + \cos\eta_0}{\sqrt{1 - \sin^2\eta_0\cos\theta}} \tag{12}$$

Combining Eq. (2) with Eq. (9) in Part 1 for the pitch p of the helical chip (under $\eta = \eta_0$), it can be shown that

$$\frac{\sin\eta_0/\tan\eta_1}{\sqrt{1 - \sin^2\eta_0\cos^2\theta}} = \frac{|p|}{2\pi\rho_0}\sqrt{\left(\frac{2\pi\rho_1}{p}\right)^2 - \tan^2\theta} \tag{13}$$

Modifying Eq. (9) in Part 1 [1] under $\eta = \eta_0$

$$\frac{\cos\eta_0}{\sqrt{1 - \sin^2\eta_0\cos^2\theta}} = \frac{|p|}{2\pi\rho_0}\sqrt{\left(\frac{2\pi\rho_0}{p}\right)^2 - \tan^2\theta} \tag{14}$$

Now it can be shown by combining Eqs. (10)–(14) that

$$k_1 - \frac{\tan|\theta|}{\rho_0}\left(|h_1| + \frac{\alpha|p|}{2\pi}\right) = 0 \tag{15}$$

where

$$\alpha = \cos^{-1}\frac{1 - k_1k_2}{\sqrt{1 - 2k_1k_2 + k_1^2}} \tag{16}$$

(where the $\cos^{-1}$ value is evaluated in the range $[0, \pi/2]$) and

$$k_1 = k_2 - \sqrt{\left(\frac{\rho_1}{\rho_0}\right)^2 - \left(\frac{p\tan\theta}{2\pi\rho_0}\right)^2} \tag{17}$$

where

$$k_2 = \sqrt{1 - \left(\frac{p\tan\theta}{2\pi\rho_0}\right)^2} \tag{18}$$

Provided that the magnitudes of ρ_0, ρ_1, $|p|$, and $|h_1|$ are given, the only unknown in Eq. (15) is $|\theta|$. Further, a numerical analysis of the equation has indicated that, for a given chip-in-hand, a unique value of $|\theta|$ is always obtained [see Fig. 8 which shows the typical variation of the expression on the left side of Eq. (15) with $|\theta|$].

Once the magnitude of $|\theta|$ has been determined, the magnitude of $|\eta_0|$ can be determined as

$$|\eta_0| = \sin^{-1}\frac{1}{\cos\theta\sqrt{1 + \left(\frac{2\pi\rho_0}{p}\right)^2}} \tag{19}$$

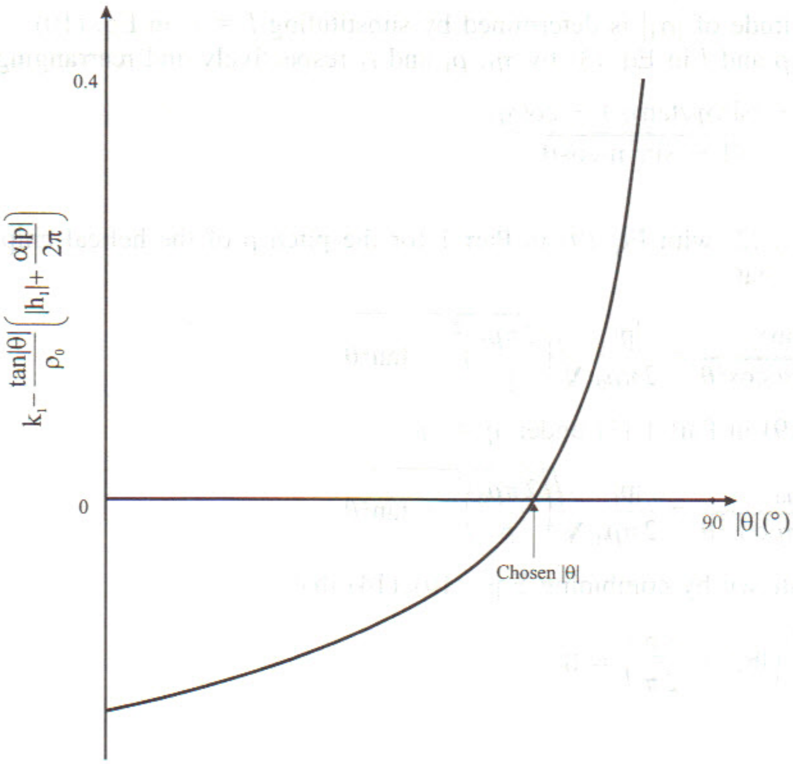

Fig. 8. Variation of $k_1 - \frac{\tan|\theta|}{\rho_0}\left(|h_1| + \frac{\alpha|p|}{2\pi}\right)$ with $|\theta|$ of the chip sample no. 1 [see Eqs. (41)–(45) of Part 1).

where the $\sin^{-1}$ value is chosen in the range [0°,90°].

As established earlier, it is a straightforward exercise to determine the values of the basic parameter set (ρ, η, θ) at any point, O, on the TCSL once the values of ρ_0, η_0 and θ have been determined. The values of ρ, η, and θ thus obtained may be substituted into Eqs. (20a) and (20b) in Part 1 to calculate the radii of up-curl and side-curl, ρ_u and ρ_s respectively, at point O.

In the above analysis, the parameter set required to be known a priori includes four easily measurable length dimensions of the chip-in-hand: ρ_0, ρ_1, $|p|$, and $|h_1|$ (see Fig. 6). Sometimes it might be more convenient to measure the slant width b_1 of the chip instead of $|h_1|$. In such cases, the magnitude of $|h_1|$ is easily determined as

$$|h_1| = \sqrt{b_1^2 + (\rho_0 - \rho_1)^2} \tag{20}$$

However, there is one case of chip when Eqs. (15)–(19) cannot be applied—the case of $|\theta| = 90°$. This case can be easily detected by the fact that the parameters of such a chip-in-hand will satisfy both the conditions $|p| = 0$ and $|h_1| = 0$. While there is no need to invoke Eqs. (15)–(18) to find $|\theta|$ when the specific case has been thus determined, the value of $|\eta_0|$ cannot be determined anyhow from the chip-in-hand parameters ρ_0, ρ_1, $|p|$, and $|h_1|$. Alternatively, it is possible that one could get an idea of how one should evaluate $|\eta_0|$ of the chip-in-hand by a study of chip formation before the chip particles arrive at the TCSL. However, a discussion of this issue is beyond the scope of the present paper. In any case, the occurrence of such a special kind of chip is quite rare in practice.

3. Experiments to demonstrate the chip-in-hand analysis

Fig. 9 shows magnified pictures of six representative chip samples. The cutting conditions under which these samples were obtained are listed in Table 1. The collection of chip samples covers a variety of cutting situations: longitudinal turning, tube turning, small (15°) and large (45°) side cutting angle, chips obtained without apparent obstruction, chips lightly obstructed through interaction with the insert clamp, and chips that have been influenced by interaction with an obstruction type chip former. Table 2 lists the results obtained from chip measurements. Table 3 lists the important geometric parameters obtained by applying the analyses presented above and in Part 1.

A study of Table 3 yields the following useful observations:

- The collection of chip samples covers a wide range of basic chip form parameters: $4° \leq \theta \leq 70°$, $-40° \leq \eta_0 \leq 47°$, and $-47° \leq \eta_1 \leq 83°$. This indicates that the analysis presented in Part 1 [1] and Part 2 (the present paper) is applicable to a wide variety of chips obtained in practice.
- Some of the chips (chips 1, 4, and 5) showed narrow creases on the side indicating that the chip material there had not assumed the chip helix parameters (helix axis, and the rotational and translational velocities about the axis) prescribed by the rigid chip model. However, the bulk of each of these chips appears to have assumed common parameters which indicates that the creasing was merely a peripheral aberration.
- δ_m/b_1 ranges from $\approx 0\%$ to 2.11%. Thus, as already noted, practical 3-D chips are only approximately conical and the error resulting from assuming that the chips are conical is small. Therefore, it is highly likely that the impact of this error on chip geometry analysis is insignificant.
- As expected, all the ρ_u-values listed are positive whereas the ρ_s-values span both negative and positive values.
- Usually, the absolute values of both ρ_u and ρ_s are significantly larger than the values of the corresponding radii, ρ_0 and ρ_1 respectively, of the chip-in-hand. This indicates that merely measuring the chip radius does not give any clue regarding the actual degree of chip-curl. One needs to further analyse the chip before any conclusion can be drawn.
- The magnitude of ρ_{u1} can be smaller or larger than that of ρ_{u0}. This observation is in agreement with formula $\rho_{u0}/\rho_{u1} = \sin 2\eta_1/\sin 2\eta_0$, which follows from Eq. (20a) in Part 1[1] and Eq. (2). Further, we have already noted that $|\eta_1| \geq |\eta_0|$ and $|\eta_1| \leq 90°$. Hence, $\rho_{u0} \geq \rho_{u1}$ when $|\eta_0|$ is small enough and, otherwise, $\rho_{u0} \leq \rho_{u1}$. This observation contradicts the commonly held simplistic belief that a single magnitude of ρ_u suffices to characterize chip up-curl.
- The absolute magnitude of ρ_{s1} is smaller than that of ρ_{s0} in *all* the cases studied. This observation is in agreement with equation $\rho_{s0}/\rho_{s1} = \sin\eta_1/\sin\eta_0$, which follows from Eq. (20b) in Part 1 [1] and Eq. (2). Therefore, the condition $|\rho_{s0}| \geq |\rho_{s1}|$ will always be satisfied (since $|\eta_1| \geq |\eta_0|$ and $|\eta_1| \leq 90°$). This observation has previously been recognized only in the context of pure 2-D side-curl.

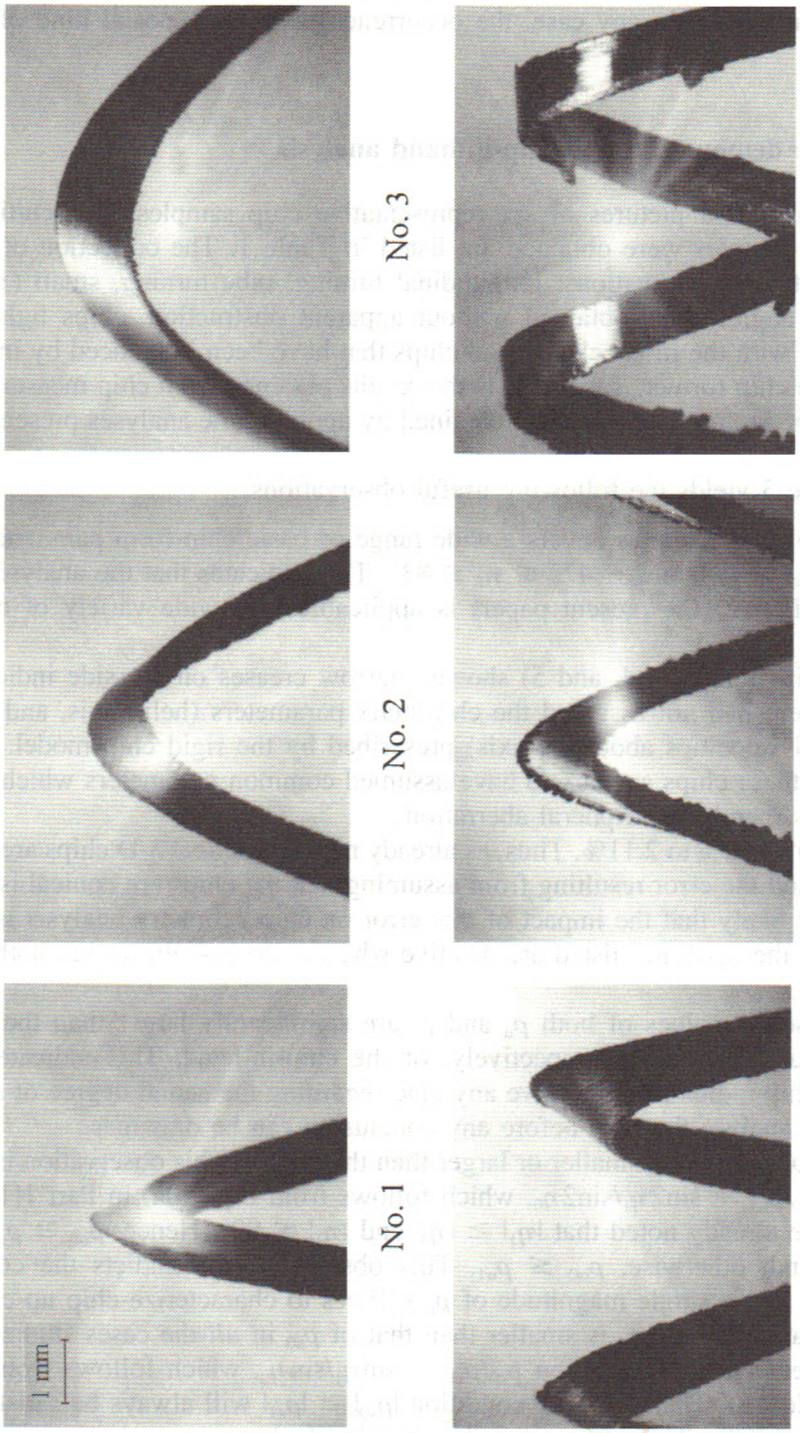

Fig. 9. Chip samples selected for analysis.

Table 1
Cutting conditions of the chip samples

Sample no.	Cutting speed (m/s)	Feed (mm/rev)	Depth (mm)	Other common features	Notes
1	1.5	0.3	0.2	Work material: steel AISI 4140 Tool insert: carbide K20 SNUN120412 Dry cutting	a
2	1.0	0.3	0.3		a,b
3	1.5	0.1	1.0		a,b,c
4	2.0	0.1	0.1		d
5	3.0	0.2	0.6		a,e
6	1.5	0.1	1.0		a,b

[a]Longitudinal turning.
[b]Tool holder CSBPR 2525K12 was turned in the reference plane to obtain a side cutting edge angle equal to 45°.
[c]The chip experienced right side-curling owing to an interaction with the insert top clamp of the tool holder.
[d]Turning of end of tube; the width of the tube wall—1 mm; special tool holder with a back rake angle and side rake angle equal to − 6° and 0° respectively; special wedge type obstruction chip breaker (the wedge angle 45°) was clamped on the tool insert rake face such that: (1) the wedge edge touched the insert face was at a distance 2.5 mm from the working cutting edge along the axis of cut which is orthogonal to the cutting edge; (2) the wedge edge was inclined to the cutting edge at an angle of 20°.
[e]Tool holder CSBPR 2525K12 was not rotated which meant that the side cutting edge angle was equal to 15°.

Table 2
Measured parameters of the chip samples

Sample no.	ρ_0 (mm)	$\Delta\rho$ (mm)	$|p|$ (mm)	$|h_1|$ (mm)
1	5.35	0.85	5.5	0.4
2	5.6	0.82	12.7	0.4
3	10.35	1.08	21.9	0.35
4	3.75	1.1	4.6	0.88
5	3.25	1.2	4.6	0.25
6	2.4	0.065	3.9	0.9

4. Conclusions

This paper (Part 2) has extended the geometric analysis presented in Part 1 [1] and has led to the following conclusions concerning steady-state 3-D chip forms obtained by cutting with tools with flat rake faces:

Table 3
Calculated parameters of the chip samples

Sample No.	1	2	3	4	5	6
θ (°)	− 63	− 58	64	50	70	− 4
η_0 (°)	− 21	− 40	47	17	40	14
η_1 (°)	− 25	− 47	54	25	83	15
l_1 (mm)	− 1.02	− 1.24	1.78	1.49	2.42	− 0.9
δ_m/b_1 (%)	0.12	0.51	0.47	0.17	2.11	< 0.001
ρ_{u0} (mm)	12.8	14.7	36.5	6.2	12.7	2.5
ρ_{u1} (mm)	11.1	14.3	38.5	4.7	52.3	2.5
ρ_{s0} (mm)	− 6.1	− 7.0	12.2	5.0	3.5	− 35.4
ρ_{s1} (mm)	− 5.1	− 6.1	11.0	3.6	2.3	− 34.5
e (mm)	1.73	3.2	7.2	0.89	2.03	− 0.04

- The geometric properties at every point on the tool–chip separation are determined once those at any one point have been determined.
- 3-D helical chips are only approximately conical. The outer surface of chips is convex in a direction away from the chip axis.
- All possible chip forms are contained within the parameter range of $90° < \eta_0 < 90°$ and $-90° \leq \theta \leq 90°$ where θ is the angle at which the chip axis meets the rake plane and η_0 is the angle between the chip velocity vector and the direction along the rake face which is normal to the tool–chip separation line. Moreover, the parameter space (η_0,θ) of the possible chips is restricted owing to the growth of the relative chip width along the TCSL, $|l_1|/\rho_0$.
- The distribution of the radii of chip up-curl and side-curl across the chip width can be determined from the results obtained from a visual inspection followed by four simple linear measurements of the chip-in-hand.

The last conclusion is of particular significance with regard to future research on chip curl. Although most practical chips are 3-D, chip curl research has so far focused on empirical and analytical studies of the 2-D cases of pure up-curl and pure side-curl. This was partly because these 2-D cases were considered to be easier to analyse and due to the absence of a methodology for determining the radii of up-curl and side-curl from simple measurements of the dimensions of the chip-in-hand. However, the analysis presented in this paper has developed a simple and straight forward method for studying 3-D chips-in-hand. Therefore, it will be useful to direct some future research on chip curl towards (i) empirically studying the behaviour of up-curl and side-curl directly from data obtained from the measurement of 3-D chips-in-hand, and (ii) developing predictive chip-curl models from the data thus obtained.

References

[1] A. Kharkevich, K.VENUVINOD Patri, Basic geometric analysis of 3-D chip forms in metal cutting. Part 1: determining up-curl and side-curl radii, International Journal of Machine Tools and Manufacture 39 (1999) 751.

[2] ISO 3685: Tool-life testing with single-point turning tools, Annex G, (1977) 41.
[3] C. Spaans, The fundamentals of three-dimensional chip curl, chip breaking and chip control. Doctor thesis, TH-Delft (1971).
[4] K. Nakayama, M. Ogawa, Basic rules on the form of chip in metal cutting, Annals of the CIRP 27 (1) (1978) 17–21.
[5] K. Nakayama, M. Arai, Comprehensive chip form classification based on the cutting mechanism, Annals of the CIRP 41 (1) (1992) 71–74.